A Sensitivity Analysis of Vibrations in Cracked Turbogenerator Units versus Crack Position and Depth

N.Bachschmid, P.Pennacchi[1], E. Tanzi
Department of Mechanical Engineering, Politecnico di Milano
Via La Masa 1, I-20156 Milan, Italy

Abstract

The dynamic behaviour of heavy, horizontal axis, turbo-generator units affected by transverse cracks can be analysed in the frequency domain by means of a quasi linear approach, using a simplified breathing crack model applied to a traditional finite element model of the shaft-line. This allows to perform a series of analyses with affordable computational efforts.
Modal analysis combined to a simplified approach for simulating the dynamical behaviour allows to predict the severity of the crack excited vibrations, resolving the old-age question on how deep a crack must be to be detected by means of vibration measurements of the machine during normal operating conditions.
The model of a 320 MW turbo-generator unit has been used to perform a numerical sensitivity analysis, in which the vibrations of the shaft-line, and more in detail the vibrations of the shafts in correspondence to the bearings, have been calculated for all possible positions of the crack along the shaft-line, and for several different values of the depth of the crack.

Keywords: Cracked rotors; rotor dynamics; sensitivity to crack depth.

1. Introduction

A very special case of damage in mechanical structures is the development and propagation of transverse cracks in rotating shafts. Transverse cracks are cracks in which the crack surface is orthogonal to the rotation axis of the shaft. The obvious difficulty in inspecting a rotating shaft during the operation of the machines makes the detection of cracks in these structures much more difficult than in static (non-rotating) structures. Therefore, symptoms are needed that can easily be measured (which are typically the vibrations) and that are able to indicate clearly the presence of a crack in a rotating shaft. If these symptoms arise in a machine, the machine can be stopped, the shaft can be removed and inspected with standard procedures and catastrophic failures of the complete set can be avoided. The accurate modelling of cracked shaft dynamical behaviour allows simulating the vibrations of a shaft affected by a transverse crack in different positions and with different depths. More in detail, the vibrations can be calculated in correspondence of the bearings of the machine, where they are measured in real machines, and its severity allows to predict the possibility of detecting the presence of the crack. A crack in rotating shafts is most likely to appear in correspondence of sharp changes of diameter or of the geometry of the shaft (presence of holes, slots for keys, threads and so on) in regions of high stress concentration.
Thermal stresses that develop in thermal machines, like steam turbines, and thermal shocks are also responsible for generating high local stress intensity factors that can cause the starting of a crack and its propagation.

[1] Contact author, phone +39.02.2399.8440, fax +39.02.2399.8492, e-mail paolo.pennacchi@polimi.it

In rotating shafts, the cracks propagate generally in a plane perpendicular to the shaft axis, when the axial bending stresses are prevailing, generating a transverse crack. The propagation velocity in a rotating shaft may change from case to case. Very frequently the crack moves by steps, alternating progresses to stops: both can be seen on the cracked surface pattern where rest lines called *beach marks* are recognizable. Generally, when the crack is approaching to a dangerous depth, it propagates more quickly, with a propagation velocity that increases exponentially, as can be deduced also by the so-called Paris law [1]. The final growth up to a critical dangerous depth takes sometimes only few days of operation. Cracks in power station and industrial plant machinery, steam turbines, generators and pumps have been discovered and documented in many European power plants as well as in the Far East and in the USA [2]-[22]. They have generally been discovered by analysing the monitored vibrations and the machines have been stopped before the occurrence of a catastrophic failure, but in some cases the symptoms have not been recognized in time and the machines burst. As far as the authors know only one published paper [23] deals with the possibility of discovering from vibration measurements the presence of cracks in 900 MW turboset units, for a *given position* of the crack and for different crack depths and circumferential extensions.
In the following the effects of transverse cracks with rectilinear tips and different depths (in this case the circumferential extensions are defined directly from the depth) that have developed in *any position* of a shaft-line are analysed.

2. Model of the breathing crack

The breathing mechanism is a result of the stress and strain distribution around the cracked area, which is due to static loads, like the weight, the bearing reaction forces and so on, and dynamical loads, like the unbalance and the vibration induced inertia force distribution. Accurate modelling of the breathing mechanism has been generally disregarded in the literature. When the static loads overcome the dynamical ones, the breathing is governed by the angular position of the shaft with respect to the stationary load direction, and the crack opens and closes again completely once each revolution. The transition from closed crack (full) stiffness to the open crack (weak) stiffness has been generally considered in literature abrupt (for the first time in [24]) or represented by a given cosine function (for the first time in [25]), but can be calculated step by step in an iterative procedure. Different approaches are compared in [26].
3D non linear finite element calculations allow the breathing mechanism to be predicted accurately, when the loads are known, but are extremely cumbersome, costly and time consuming (due to the need of a refined mesh in the crack region and to the non-linear contact conditions).
A simplified model, which assumes linear stress and strain distributions, for calculating the breathing behaviour, has been developed by the authors and proved to be very accurate [26]. The determination of the breathing behaviour is a non-linear iterative procedure. The breathing mechanism is affected also by transient thermal stresses, which can arise in rotating shafts during a change in operating conditions, and by pre-stresses, which can develop during the crack propagation. These pre-stresses can further open the crack or can tend to hold the crack more closed, influencing the breathing behaviour (as described in [27]). Also these aspects have been generally completely disregarded in previous investigations.
The proposed model is as follows: the initial position of the main inertia axes of the supposedly partially open crack surface is assumed as well as a linear axial stress distribution due to the bending load to which eventually also thermal stresses are superposed. Then the compressive and tensile stresses are defined: cracked surfaces where tensile stresses should appear are “open” areas, where compressive stresses appear are “closed” areas (see figure 1).

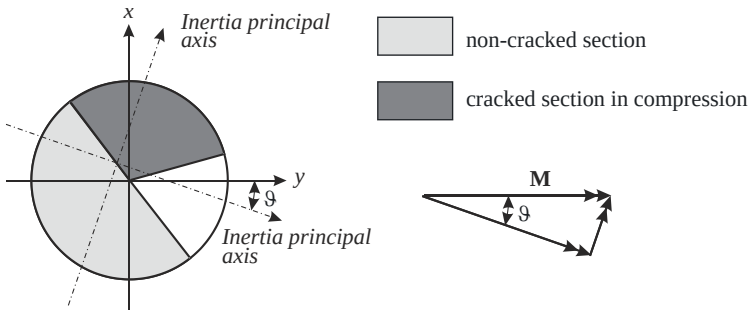

Figure 1. Main axis of inertia and the bending moment decomposition in a generic position of the cracked section.

Indeed open and closed areas define also the main inertia axes position. Therefore the procedure has to be repeated iteratively, until the position of the main axes remains stable.
With this simplified model accurate results have been found, despite the fact that the proposed approach assumes linear stress distribution where in reality the stress distribution is strongly non-linear, as it is well known from Fracture Mechanics and from 3D finite element non-linear analyses.
Once the breathing mechanism and the second moments of area have been defined for the different angular positions of the cracked section, the stiffness matrix of an *equivalent* cracked beam element of suitable length l_c can be calculated, assuming a Timoshenko beam with constant section and second moments of area along l_c, as shown in figure 2, for each different angular position. The neighbour beam elements are again circular section beams. The angular position dependent stiffness matrix $\mathbf{K}_c(\Omega t)$ is one per revolution periodical, has one constant term (the mean stiffness) and several harmonic components of which only the first three components are significant.

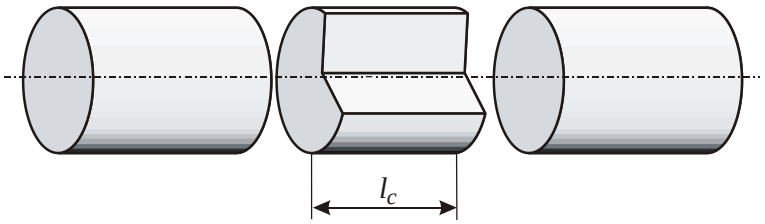

Figure 2. Equivalent cracked beam element: its configuration changes with its angular position.

The stiffness matrix (square, symmetrical, 8×8 elements) is represented in eq. (1):

$$\left[\mathbf{K}_c(\Omega t)\right]\begin{Bmatrix}\mathbf{x}_1\\ \mathbf{x}_2\end{Bmatrix}=\begin{bmatrix} a & c & p & q & -a & c & -p & q \\ & e & -q & r & -c & f & q & s \\ & & b & -d & -p & -q & -b & -d \\ & & & h & -q & s & d & g \\ & & & & a & -c & p & -q \\ & & & & & e & q & r \\ & & & & & & b & d \\ & & & & & & & h \end{bmatrix}\begin{Bmatrix} x_1 \\ \vartheta_{y1} \\ y_1 \\ \vartheta_{x1} \\ x_2 \\ \vartheta_{y2} \\ y_2 \\ \vartheta_{x2} \end{Bmatrix} \tag{1}$$

where the coefficients are defined as:

$$a=\frac{12\,J_y\,E}{(1+\phi)\,l_c^3},\ b=\frac{12\,J_x\,E}{(1+\phi)\,l_c^3},\ c=\frac{6\,J_y\,E}{(1+\phi)\,l_c^2},\ d=\frac{6\,J_x\,E}{(1+\phi)\,l_c^2},\ e=\frac{(4+\phi)\,J_y\,E}{(1+\phi)\,l_c},$$
$$f=\frac{(2-\phi)\,J_y\,E}{(1+\phi)\,l_c},\ g=\frac{(2-\phi)\,J_x\,E}{(1+\phi)\,l_c},\ h=\frac{(4+\phi)\,J_x\,E}{(1+\phi)\,l_c},\ p=\frac{12\,J_{xy}\,E}{(1+\phi)\,l_c^3}, \tag{2}$$

$$q = \frac{6 J_{xy} E}{(1+\phi) l_c^2}, r = \frac{(4+\phi) J_{xy} E}{(1+\phi) l_c}, s = \frac{(2-\phi) J_{xy} E}{(1+\phi) l_c}, \phi = \frac{12 E J}{G S l_c^2}$$

The parameter ϕ accounts for the shear effects, E and G are respectively the Young's modulus and the shear modulus, S is the reduced cross section area, J_x, J_y, J_{xy} are the reduced second moments of area.

Figure 3 shows the reference frame for the 6 degrees of freedom and the static loads commonly present in rotating shafts: the bending moment M_b and the torsion M_t. In the present analysis only 4 degrees of freedom are used (torsion and axial displacements are not considered) for evaluating the flexural bending behaviour and possible effects of torsion on bending behaviour and vice versa are neglected.

Note that the stiffness coefficients are all proportional to the corresponding second moments of area which are functions of the depth and of the angular position Ωt since they depend on the 1X periodical breathing of the crack. The length l_c depends on the depth only and has been tuned by 3D finite element calculations, comparing the deflections of a cracked beam element loaded by bending and torsion in different angular positions with those calculated using the proposed model. In [26] it has been shown that a constant l_c for all angular positions of the crack provides optimum fitting with 3D results. Its dimensionless length (length l_c divided by the depth a of the crack) is shown in figure 4 as function of the dimensionless depth a/D (depth a divided by the diameter D of the shaft). In this figure and in the following analysis the crack has always been assumed with rectilinear tip.

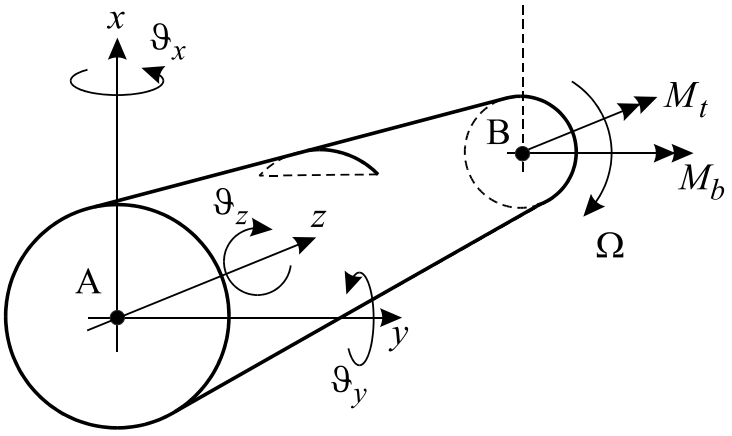

Figure 3. Cracked beam reference frame.

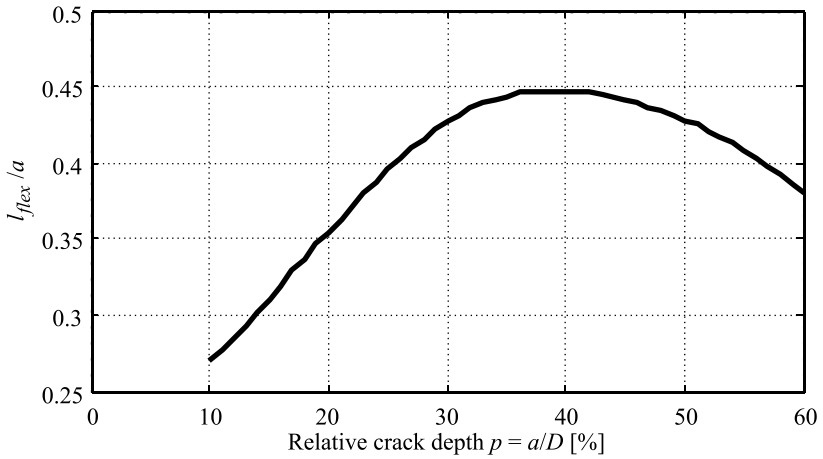

Figure 4 Dimensionless length l_c/a as function of dimensionless depth $p = a/D$.

3. Dynamical behaviour of cracked shafts

When the equivalent cracked beam having a reduced cross section and a suitable length is inserted in the 1D standard rotor-dynamic FEM of the rotor, the global stiffness matrix including bearing and supporting structure stiffness, which, due to the presence of the breathing crack, is once per revolution (1X) periodical, can be expanded in a Fourier series according to eq. (3).

$$[\mathbf{K}(\Omega t)] = [\mathbf{K}_m] + \sum_j [\Delta \mathbf{K}_j] \mathrm{e}^{\mathrm{i}\, j\Omega t},\ j = 1,2,3 \tag{3}$$

The Fourier expansion of the periodic stiffness matrix is truncated at the third harmonic component. Each component depends on the crack depth only. The equation of motion of the rotor can be expressed with eq. (4),

$$[\mathbf{M}]\ddot{\mathbf{x}} + ([\mathbf{C}] + [\mathbf{Gyr}]\Omega)\dot{\mathbf{x}} + \left([\mathbf{K}_m] + \sum_j [\Delta \mathbf{K}_j] \mathrm{e}^{\mathrm{i}\, j\Omega t} \right) \mathbf{x} = \sum_n \mathbf{F}_{e_n} \mathrm{e}^{\mathrm{i}\, n\Omega t} + \mathbf{W},\ j = 1,2,3 \tag{4}$$

where **W** is the weight force vector and $\mathbf{F}_e$ the vector that contains both the exciting forces acting on the rotor (e.g. unbalances) and the resultant moments of the thermal stress distribution acting on the cracked section. **M** is the mass matrix of the system (including the supporting structure), **C** and **Gyr** are respectively the damping and gyroscopic matrices. The rotor displacements **x** can be split in their static and dynamic components $\mathbf{x}_s$ and $\mathbf{x}_d$:

$$\mathbf{x} = \mathbf{x}_s + \mathbf{x}_d \tag{5}$$

where

$$\mathbf{x}_s = [\mathbf{K}_m]^{-1} \left(\mathbf{W} + \mathbf{F}_0 \right) \tag{6}$$

$\mathbf{F}_0$ is a static force vector defined below in eq. (13) due to the presence of the crack.
Then, eq. (4) can be rewritten in the following form:

$$[\mathbf{M}]\ddot{\mathbf{x}}_d + ([\mathbf{C}] + [\mathbf{Gyr}]\Omega)\dot{\mathbf{x}}_d + [\mathbf{K}_m]\mathbf{x}_d = \sum_n \mathbf{F}_{e_n} \mathrm{e}^{\mathrm{i}\, n\Omega t} - \sum_j [\Delta \mathbf{K}_j] \mathrm{e}^{\mathrm{i}\, j\Omega t} \left(\mathbf{x}_s + \mathbf{x}_d \right),\ j = 1,2,3 \tag{7}$$

The last term of equation (7) represents the so-called *equivalent crack forces* that excite the vibrations of the shaft-line with stiffness $\mathbf{K}_m$, which is the mean stiffness of the system. The mean stiffness $\mathbf{K}_m$ (which accounts for the mean reduction due to the breathing crack) is only slightly different from the stiffness of the un-cracked shaft, as can be deduced from static deflection calculation or from modal stiffness evaluation analysing the natural frequencies.
If only the steady state solution due to the exciting forces is of interest, being the exciting forces periodical, then it is possible to shift from time domain to the frequency domain.
Let $\mathbf{F}_j$ indicate the j-th component of the forces due to the crack and $\mathbf{F}_{t_j}$ that of the total forces:

$$\mathbf{F}_{t_j} \mathrm{e}^{\mathrm{i}\, j\Omega t} = \mathbf{F}_{e_j} \mathrm{e}^{\mathrm{i}\, j\Omega t} + \mathbf{F}_j \mathrm{e}^{\mathrm{i}\, j\Omega t},\ j = 1,2,3 \tag{8}$$

The vibrations $\mathbf{x}_d$ in steady state conditions are also periodical and can be expanded in a Fourier's series:

$$\mathbf{x}_d = \sum_j \mathbf{x}_j \mathrm{e}^{\mathrm{i}\, j\Omega t},\ j = 1,2,3 \tag{9}$$

where $\mathbf{x}_1$, $\mathbf{x}_2$ and $\mathbf{x}_3$ are 1X, 2X and 3X complex harmonic vibration components, respectively.
By applying the harmonic balance approach to eq. (7), the following equations are obtained:

$$\left(-(j\Omega)^2[\mathbf{M}]+\mathrm{i}\ j\Omega([\mathbf{C}]+[\mathbf{Gyr}]\Omega)+[\mathbf{K}_m]\right)\mathbf{X}_j=\mathbf{F}_{t_j},\ j=1,2,3 \tag{10}$$

Then, the equivalent crack forces (and moments) $\mathbf{F}_j$ given by eqs. (13)-(16) applied at the nodes of the equivalent cracked beam element are calculated by substituting eqs. (11) and (12) into the last term of eq. (7).

$$\mathrm{Re}\left(\mathbf{x}_j\,\mathrm{e}^{\mathrm{i}\,j\Omega t}\right)=\frac{1}{2}\mathbf{x}_j\,\mathrm{e}^{\mathrm{i}\,j\Omega t}+\frac{1}{2}\mathbf{x}_j{}^{*}\,\mathrm{e}^{-\mathrm{i}\,j\Omega t},\ j=1,2,3 \tag{11}$$

$$[\Delta\mathbf{K}_j]\mathrm{e}^{\mathrm{i}\,j\Omega t}=\frac{1}{2}[\Delta\mathbf{K}_j]\mathrm{e}^{\mathrm{i}\,j\Omega t}+\frac{1}{2}[\Delta\mathbf{K}_j]^{*}\,\mathrm{e}^{-\mathrm{i}\,j\Omega t},\ j=1,2,3 \tag{12}$$

$$\mathbf{F}_0=\frac{[\Delta\mathbf{K}_1]}{4}\mathbf{x}_1^{*}+\frac{[\Delta\mathbf{K}_1]^{*}}{4}\mathbf{x}_1+\frac{[\Delta\mathbf{K}_2]}{4}\mathbf{x}_2^{*}+\frac{[\Delta\mathbf{K}_2]^{*}}{4}\mathbf{x}_2+\frac{[\Delta\mathbf{K}_3]}{4}\mathbf{x}_3^{*}+\frac{[\Delta\mathbf{K}_3]^{*}}{4}\mathbf{x}_3 \tag{13}$$

$$\mathbf{F}_1\,\mathrm{e}^{\mathrm{i}\Omega t}=\left([\Delta\mathbf{K}_1]\mathbf{x}_s+\frac{[\Delta\mathbf{K}_2]}{2}\mathbf{x}_1^{*}+\frac{[\Delta\mathbf{K}_3]}{2}\mathbf{x}_2^{*}+\frac{[\Delta\mathbf{K}_1]^{*}}{2}\mathbf{x}_2+\frac{[\Delta\mathbf{K}_2]^{*}}{2}\mathbf{x}_3\right)\mathrm{e}^{\mathrm{i}\Omega t} \tag{14}$$

$$\mathbf{F}_2\,\mathrm{e}^{\mathrm{i}2\Omega t}=\left([\Delta\mathbf{K}_2]\mathbf{x}_s+\frac{[\Delta\mathbf{K}_3]}{2}\mathbf{x}_1^{*}+\frac{[\Delta\mathbf{K}_1]}{2}\mathbf{x}_1+\frac{[\Delta\mathbf{K}_1]^{*}}{2}\mathbf{x}_3\right)\mathrm{e}^{\mathrm{i}2\Omega t} \tag{15}$$

$$\mathbf{F}_3\,\mathrm{e}^{\mathrm{i}3\Omega t}=\left([\Delta\mathbf{K}_3]\mathbf{x}_s+\frac{[\Delta\mathbf{K}_1]}{2}\mathbf{x}_2+\frac{[\Delta\mathbf{K}_2]}{2}\mathbf{x}_1\right)\mathrm{e}^{\mathrm{i}3\Omega t} \tag{16}$$

where $\mathbf{x}_j^{*}$ and $[\Delta\mathbf{K}_j]^{*}$ are conjugate complex quantities of $\mathbf{x}_j$ and $[\Delta\mathbf{K}_j]$.

The main components of the above force vectors are the moments according to the vertical and horizontal coordinates rather than the forces. The static and dynamic response of the cracked rotor can be evaluated using eq. (10) that is solved with an iterative procedure, shown in the flowchart of figure 5 for the three harmonic components, by considering the force vectors obtained with eqs. (13)-(16).

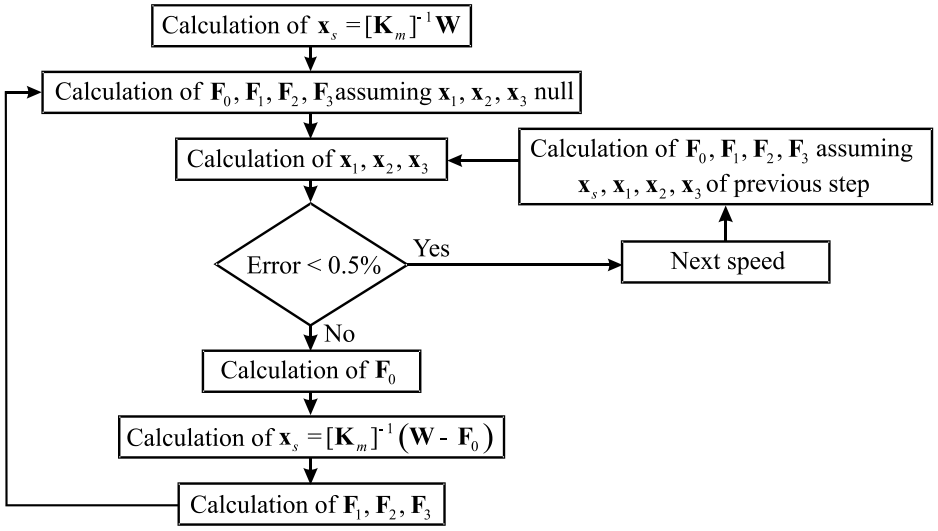

Figure 5. Flow chart of the iterative procedure used to evaluate the dynamic response of the cracked rotor.

In this linear approach, only the static bending moment is considered, because the bending moment due to the inertia force distribution associated to the rotor vibrations usually gives a small contribution in respect to the static bending moment (often only near the rotor critical speeds it can become significant). This assumption is generally acceptable for heavy horizontal rotating machines.
The crack effect on the bending stiffness is much higher than that one on the shear stiffness as it is shown in [28], where shear effects are evaluated. Thus, it results that the *equivalent force vector* $\mathbf{F}_j$ defined by eqs. (14)-(16) is composed mainly by *bending moments* (given by bending stiffness $[\Delta\mathbf{K}_j]$ of the cracked beam element, multiplied by the angular deflections $\mathbf{x}_j$ of the end nodes of the cracked element, or by its curvature).
In other words the *equivalent crack forces*, which excite in the un-cracked shaft with mean stiffness $[\mathbf{K}_m]$ the vibrations that are caused by the crack in the cracked shaft, are proportional to the different harmonic components $[\Delta\mathbf{K}_j]$of the crack dependent bending stiffness variation, multiplied by the static $\mathbf{x}_s$ and dynamic $\mathbf{x}_j$ *curvatures* of the cracked beam element. The static curvature $\mathbf{x}_s$ of the cracked element of length l_c is proportional to the static bending moment $\mathbf{M}_b$ and inversely proportional to the second moment of area of the shaft section (which means to fourth power of the shaft diameter), multiplied by l_c which is proportional to the shaft diameter D. Therefore $\mathbf{x}_s$ is proportional to the ratio of bending moment $\mathbf{M}_b$ to the third power of shaft diameter D:

$$\mathbf{x}_s \propto \frac{\mathbf{M}_b}{D^3} \tag{17}$$

Also the dynamic curvatures $\mathbf{x}_j$ caused by the crack are proportional to the static bending moment, divided by the third power of the diameter, as can be seen developing the iterative procedure. Since the vibrations $\mathbf{x}_j$ are caused not only by the crack but also by other exciting causes (like unbalance, bow and so on), the equivalent crack forces may be modified by the presence of vibrations excited by other causes, but this modification is generally small and can be neglected in a first approximation. Therefore it results that the equivalent crack forces are proportional to the static curvature of the cracked beam:

$$\mathbf{F}_j \propto \mathbf{x}_s \tag{18}$$

It is possible to say that the equivalent crack forces of eqs. (14)-(16) impose additional deflections (see figure 6) to the shaft that in reality are generated by the periodical additional bending flexibility introduced by the breathing crack in the cracked element. The equivalent rotating crack force vector is composed by pairs of bending moments, applied to the end nodes of the cracked beam element, which generate the additional bending deflections of the cracked element. These crack forces are proportional to the static non-rotating bending moment, divided by the third power of shaft diameter.
When the crack is located in a position along the shaft where the static bending moment is small (for instance close to bearings) the excitation of vibrations is weak. When instead it is located where the static bending moment is large (at midspan between bearings) the excitation is much stronger, for a given constant shaft diameter. When also the shaft diameter variations are considered, then maximum excitation is found when the crack is located in positions where the ratio of bending moment to third power of diameter is maximum, as will be shown also in following numerical simulation.
Moreover, the excitation of each harmonic component is proportional to the corresponding stiffness variation $[\Delta\mathbf{K}_j]$ (see eqs. (14)-(16)), which is in turn proportional to the variation of the second

moments of area ΔJ_j over the equivalent length l_c, which are both *function of the crack depth only*, as can be deduced from the structure of $[\mathbf{K}_c(\Omega t)]$ in eq. (2):

$$[\Delta \mathbf{K}_j] \propto \frac{\Delta J_j}{l_c} \tag{19}$$

Summarizing, the crack forces that excite the vibrations due to crack, depend on *crack depth* only and are proportional to the ratio of *static bending moment* to the *third power of shaft diameter*.

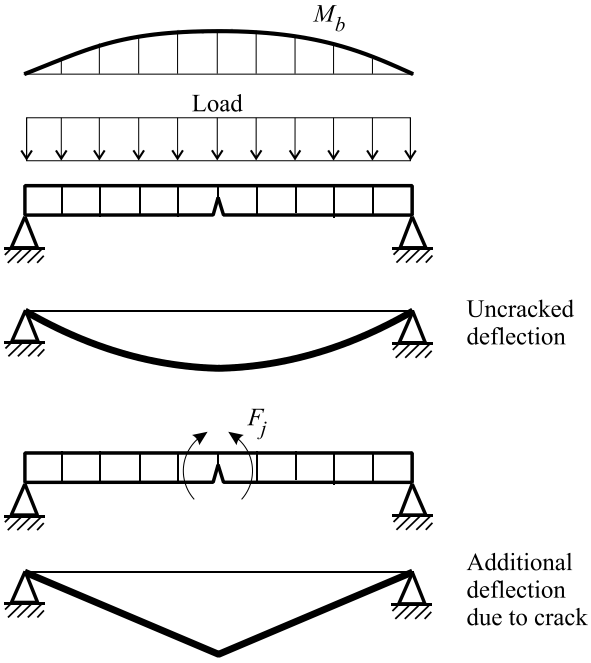

Figure 6. Additional deflections due to the crack.

4. Evaluation of vibration components excitation as function of crack depth

The effect of the full expressions of the equivalent crack forces eqs. (14)-(16) is evaluated by calculating the first three harmonic vibration components for different crack depths. The model of a simple symmetrical shaft affected by a crack with rectilinear tip located at mid-span between the two bearings is used for analysing the dependence of vibration excitation on crack depth. The vibration amplitudes for different crack depths are calculated at mid-span of the shaft at very low rotating speed, in order to avoid any dynamic effect. The amplitudes excited are divided by the mean static deflection in the same position, in order to get the dimensionless trend of vibration excitation as function of the depth.

The simple model is shown in figure 6. The shaft is loaded by its own weight only. The diagram over the shaft shows the resulting bending moment and the diagram under the shaft represents the static deflection shape, from which also the beam curvature in the different positions can be evaluated.

Figure 7 shows the first three harmonic component amplitudes as a function of the crack depth.

These dimensionless ratios are independent of the used shaft model and give an idea on how the vibration components increase as the crack propagates deeper.

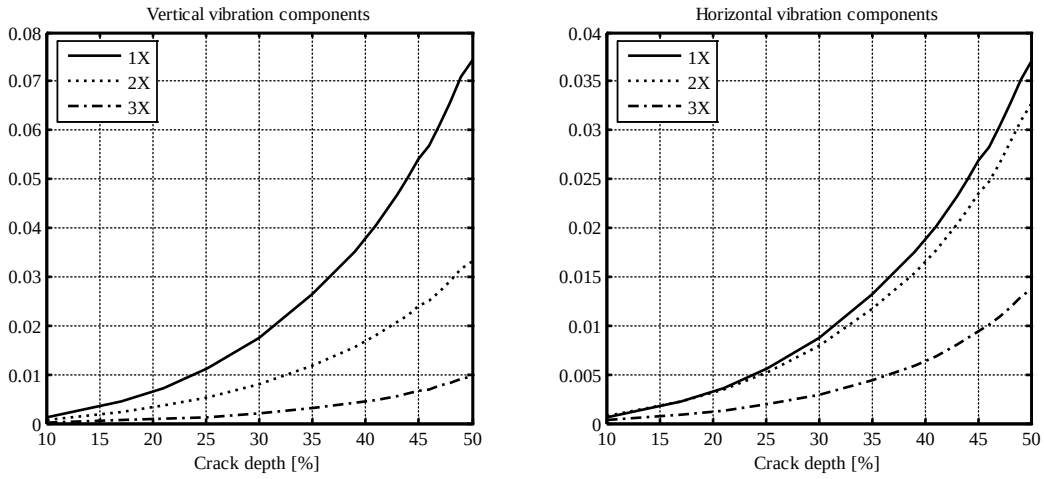

Figure 7. Crack induced dimensionless vibration components x_n/x_s versus crack depth.

The 1X excitation is higher (roughly double) in vertical direction than in horizontal direction, 2X is almost equal in both directions, 3X is slightly higher in horizontal direction than in vertical direction, for any depth. So the trend of vibration excitation of the different harmonic components as function of the depth can be forecasted.

The response of the rotating shaft to the vibration excitation depends obviously on the rotating speed dependent dynamical behaviour of the shaft and on the position where the equivalent crack forces are applied. This will be shown with the aid of a model of a turbogenerator unit.

5. Sensitivity analysis for a typical turbogenerator unit

Figure 8 shows the FE model of a 320 MW a turbogenerator unit composed by a HP-IP steam turbine, a LP steam turbine and a generator. The unit is equipped with 7 oil-film bearings, which are modelled by their linearized stiffness and damping coefficients. The supporting structure is modelled by means of simple pedestals.

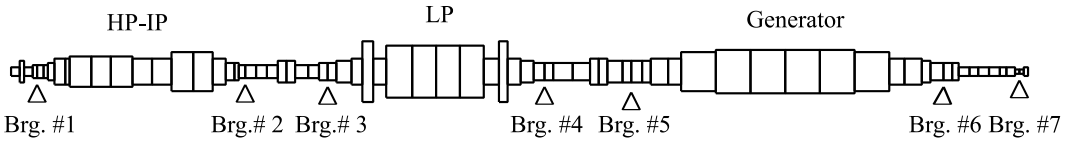

Figure 8. Finite element model of a turbogenerator unit.

Let us now examine the static bending moment distribution along the shaft-line with reference to this typical unit. This analysis, along with the evaluation of the shaft diameters in the different positions along the shaft-line allows understanding where and when crack excitation can be either severe or weak.

The actual static bending moment, which is responsible for generating the crack forces and the related vibrations, depends on the distribution of masses along the shaft-line and on the bearing alignment conditions. Generally the first alignment in cold conditions is made by imposing null forces and moments in correspondence of the coupling flanges of the different shafts. With respect to this situation some change may be introduced with the aim of increasing loads on bearings which, being lightly loaded, could operate close to its instability threshold. This occurs e.g. in the 320 MW turbogenerator of figure 8 for the last bearing of the generator (bearing #7). At the operating speed, this alignment condition is slightly modified by the oil film thickness that builds up in the different bearings and displaces the journals. In some machines also the thermal expansion of the supporting structure may modify the initial alignment conditions. In order to simulate accurately the effect of a crack the actual static bending moment distribution in operating conditions

should be considered. Figure 9 shows the comparison between the distributions of the static bending moments in the vertical and in the horizontal plane at rest and at the normal operating speed of 3000 rpm. The two curves are superposed and differences are negligible in the vertical direction. The differences are recognizable (due to different scales) only in horizontal direction. At rest, the horizontal bending moments are null, when the alignment in this direction is according to a straight line (as it should theoretically be). At the operating speed, they are due to the oil film which builds up in the bearings and displaces the journals. It can be seen that the bending moments in horizontal direction are negligible with respect to the bending moments in vertical direction in almost all positions along the shaft-line except in positions close to the bearings where the vertical bending moments become very small.

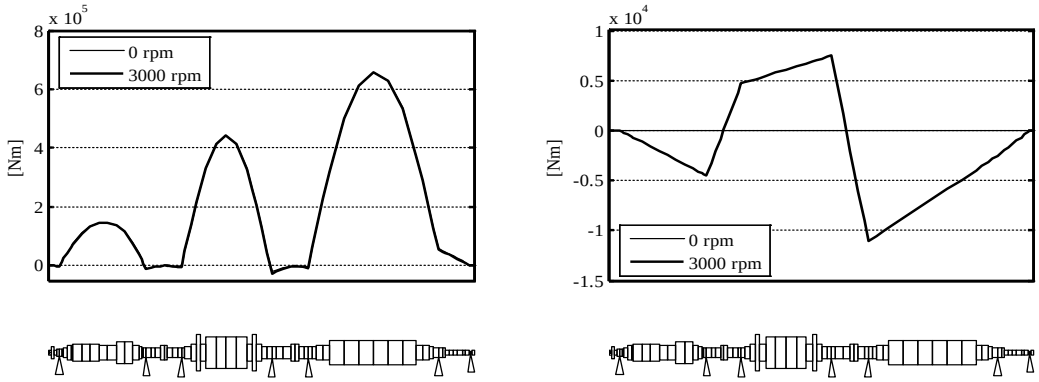

Figure 9. Static bending moments distributions along the shaft-line at rest and at normal operating condition: left in vertical plane and right in horizontal plane.

Bearing in mind that the crack forces are proportional to $\mathbf{x}_s$ that is proportional in each node to the static bending moment, divided by the third power of shaft diameter, see eq. (17), it results that cracks generate maximum excitation when they are located close to the mid-span of shafts with diameters which are not changing abruptly (like in the HP-IP steam turbine) or when they are located in a different position where the bending moment is still rather high, and the shaft diameter is rather low (as it occurs in the LP steam turbine close to the two symmetrical last blade stages, indicated by the two disks in the FE model).

The natural frequencies (eigenfrequencies) and the associated mode shapes (eigenvectors) have been calculated at the operating speed of 3000 rpm. The most significant mode shapes and associated frequencies and damping factors are shown in figure 10. Some highly damped modes have been disregarded. The first six modes correspond to classical modes of single shafts:

- Modes I, II and III correspond respectively to the first bending modes of the generator, of the LP turbine and of the HP-IP turbine shafts.
- Modes IV, V, and VI are respectively a different first mode of the HP-IP turbine shaft, the second mode of the LP turbine and the second mode of the generator shafts.
- Mode VII is another generator shaft second mode.
- Mode X is displayed to show that in the higher frequency range (close to 2X excitation) mode shapes present high amplitudes in parts of the shaft-line in between adjacent bearings, where couplings are present or where the exciter of the generator is located.

All these mode shapes should be taken into consideration when the generalized crack forces for the different mode shapes are estimated. Being the crack forces equivalent to bending moments applied locally, their generalized forces are strong (which means that the energy introduced by the equivalent bending moments in that particular vibration mode is large), when the crack is located in a position where the mode shape presents high curvature.

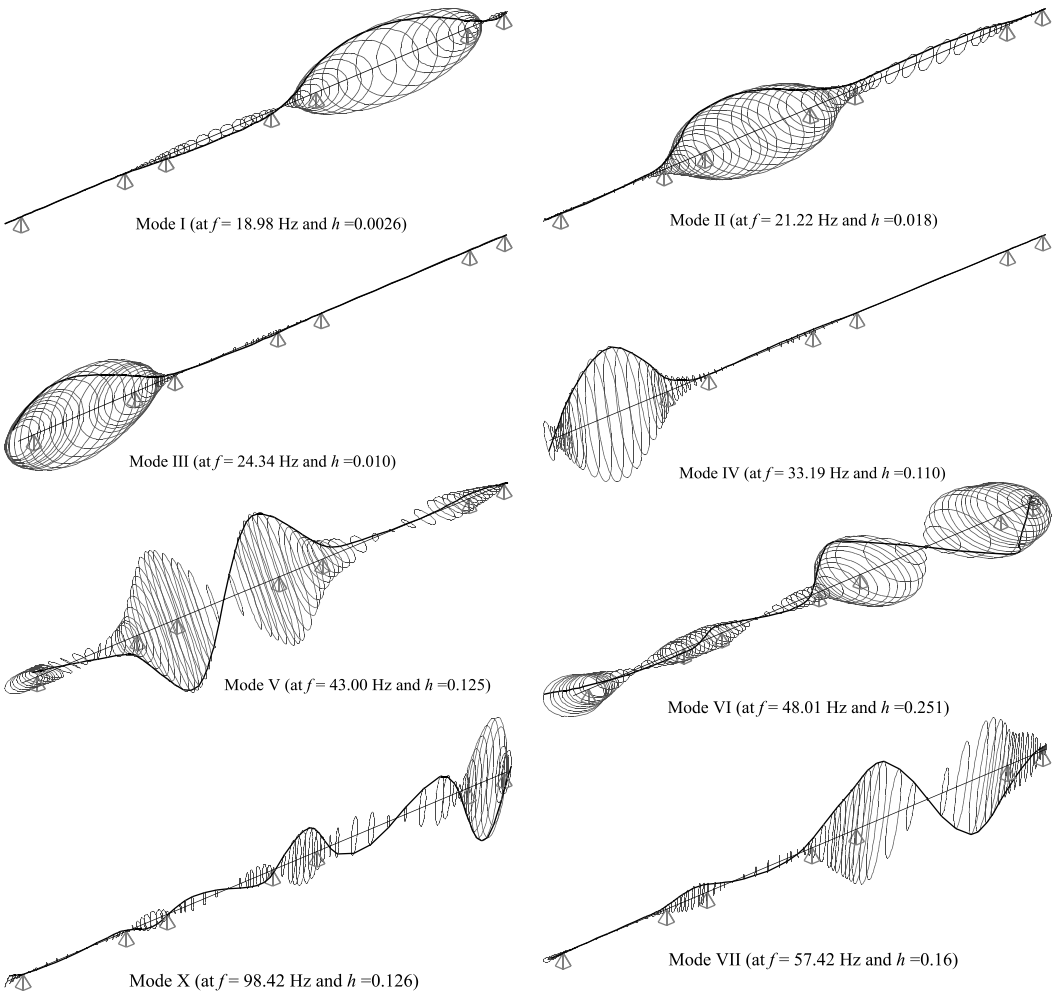

Figure 10. Most significant mode shapes and damping factors h of the turbogenerator unit.

Cracks at mid-span of single shafts excite strongly their first bending modes when the shaft is rotating at the corresponding frequency (critical speed), but excite very weakly their second bending modes. These are more strongly excited when the crack is located closer to the main bearings (see modes V and VI of figure 10). The closest mode to the running speed frequency (mode VI) is the second mode of the generator that could be strongly excited by a crack located on the shaft close to its main bearings, considering only the 1X component of the exciting force. Its 2X component at running speed would excite the generator shaft vibrations of mode X more strongly if the crack would have developed in positions close to bearing #6.

The presence of a transverse crack will affect only slightly the natural frequencies and the associated mode shapes.

This will be shown in the following example: a crack with two different depths (25% and 50% of the diameter) has been applied in the mid-span of the LP turbine rotor, in order to maximize its influence on the first bending critical speed. Figure 11 shows the frequency response curves calculated in bearing #3 of the unit for the un-cracked shaft, excited by a given unbalance, and for the cracked shaft excited by crack only. Resonance peaks at first bending critical speed are found at 1460 rpm for the un-cracked shaft, 1450 rpm for the shaft affected by the small crack (25%) with a frequency shift of 0.6% and at 1414 rpm for the shaft affected by the large crack (50%) with a frequency shift of 3.15%. Note that the natural frequency has moved from the eigenfrequency of 21.22 Hz calculated at rated speed of 3000 rpm (see figure 10) to 24.33 Hz (1460 rpm) due to the higher oil film stiffness at lower rotating speeds.

The same cracks in different positions of the same shaft will produce smaller frequency shifts, which can also vanish completely. This confirms the well known opinion that small cracks may not

sufficiently affect the bending critical speeds of shafts, so that frequency shifts cannot be considered a consistent symptom of their presence. Bending modes are generally well damped: resonance peaks are very smooth and this fact increases the difficulty of measuring critical frequency shifts in real machines.
Differences of mode shapes would be probably higher, but they have not been taken into considerations due to the difficulties, or the practical impossibility, of measuring the mode shapes in real machines during operating conditions.

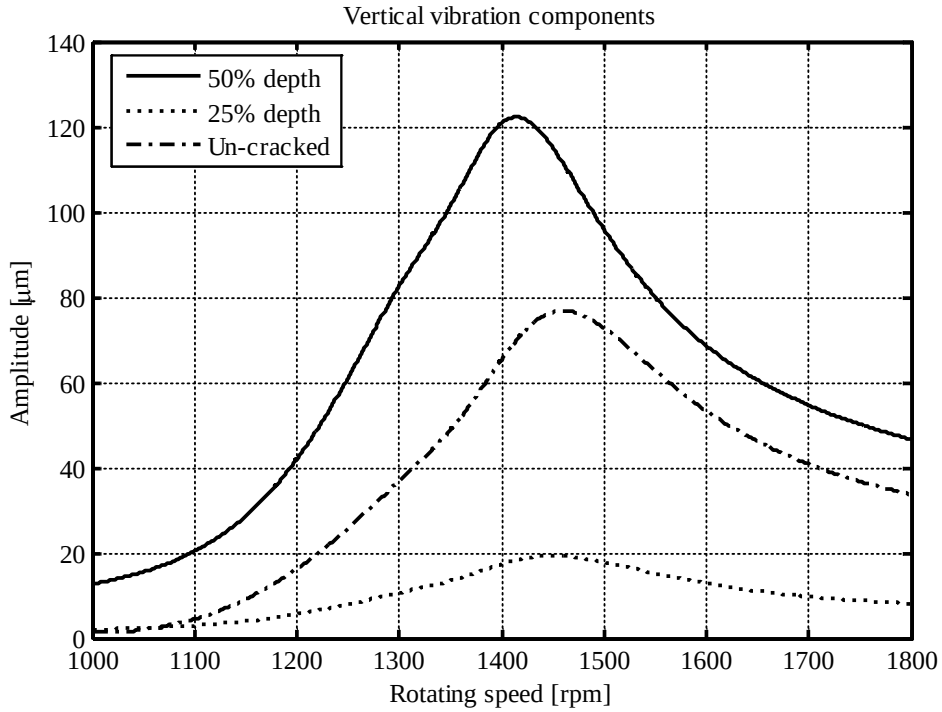

Figure 11 - Frequency response curves in bearing #3 of the turbogenerator unit for cracks located at mid-span of the LP turbine rotor, compared to un-cracked shaft behaviour

A numerical analysis has been performed by calculating the vibration behaviour of the unit affected by transverse cracks only for two different depths in different positions along the shaft: a rather small crack with depth of 25% of the diameter and a rather deep one of 50% of the diameter. The cracks have been located successively into all the elements of the shaft-line. The waterfall diagrams show the deflections along the shaft-line as a function of the different crack locations. For clarity reasons all the deflections between the bearings are not displayed, in order to highlight the vibrations in correspondence of the bearings only.
Figures 12 and 13 show the waterfall plots of respectively the 1X and 2X vibrations in the bearings in vertical direction as a function of the crack position for a crack with depth of 25% of the diameter. 1X vibration excitation is larger in vertical than in horizontal direction, which is not shown for brevity. 2X vibration excitation is instead almost equal in horizontal and vertical direction. Both results were predicted in figure 7. The maximum 1X vibration amplitude in bearings #1 and #2 is less than 4 μm when the crack is located between the HP and the IP sections of the turbine, position in which the vibration excitation is maximum.
In bearings #3 and #4 the maximum amplitude is about 10 μm when the crack is located in positions of the LP turbine close to one or the other elements modelling the last stages, where the vibration excitation is maximum. High dynamic response is expected for cracks in these positions, bearing in mind the LP turbine mode shape at 43 Hz (mode V of figure 10 that is rather close to 50 Hz) and the high curvatures. On the generator, the maximum amplitude is about 9 μm in bearing #5 when the crack is located on the generator in a position rather close to bearing #6, where the shaft diameter has a strong reduction.

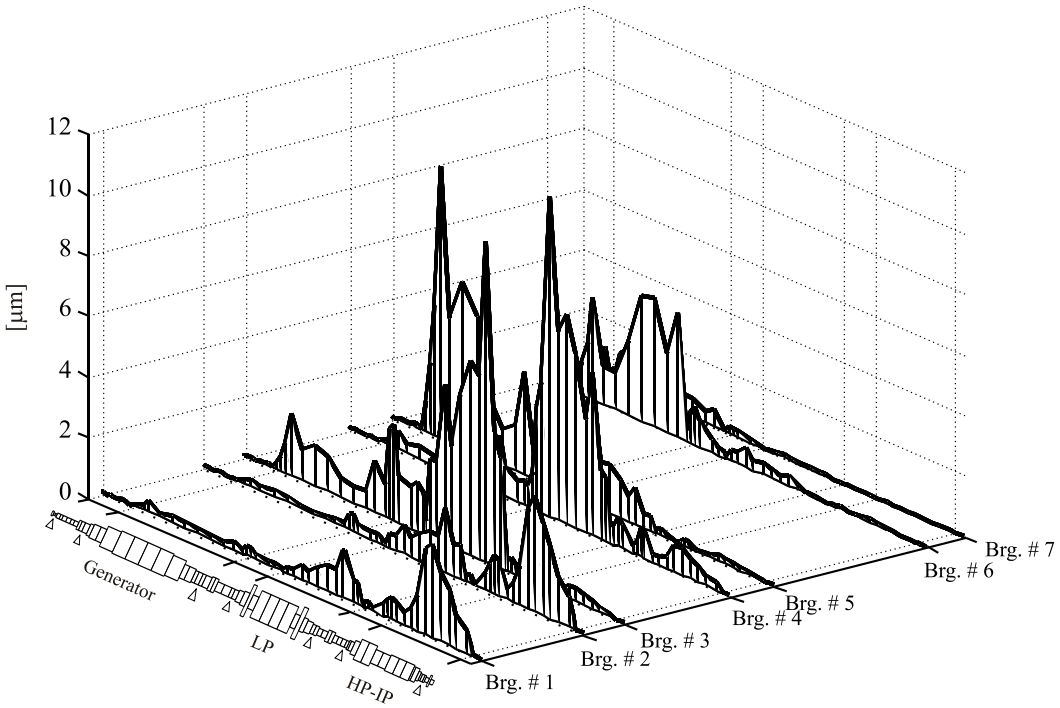

Figure 12. Waterfall plot of 1X vertical vibration amplitudes in correspondence of the bearings (at operating speed of 3000 rpm) as a function of the position of a 25% deep crack.

In this position the excitation is strong due to a good ratio of bending moment to diameter, as also in the symmetrical position close to bearing #5, but the response due to excitation close to bearing #6 is higher in bearing #5 than the response in bearing #6 due to the same excitation. The response in bearing #6 due to excitation in bearing #5 is lower. This can be explained considering the effect of the dynamical behaviour of the unit at the frequency of 50 Hz, which is between the natural frequencies at 48.01 and 57.42 Hz where the modes VI and VII of figure 10 show high curvatures in the shaft close to bearing #6 (in mode VI) and high vibration amplitudes in bearing #5 (in mode VII).

Figure 13 shows that the maximum 2X vibration amplitudes in bearings #1 and #2 are less than 2 μm when the crack is between the HP and the IP sections of the turbine (maximum excitation), less than 3 μm in bearings #3 and #4 when the crack is in the LP turbine close to one of the last stage elements (again in positions of maximum excitation). In both cases the response is not very high as can be deduced from mode shape X at the frequency of 98.42 Hz, which shows low vibration levels in both turbines. In bearing #5 a maximum of 4.6 μm is found when the crack is on the generator, in a position close to bearing #6. The crack in the same position excites also 3.5 μm in bearings #6 and #7. These effects are due to the dynamical behaviour of the group at the frequency of 100 Hz, when the excited vibration mode is close to the mode shape X. High curvature of the mode shape in correspondence of the crack position and high vibration amplitudes in correspondence of bearing #5 justify the calculated behaviour.

The 2X excitation is roughly half the 1X excitation, as predicted in figure 7 , but dynamic effects are different at 50 and 100 Hz. The 2X component, which is the most reliable symptom related to a developing crack, is rather small for the 25% deep crack and could hardly be detected by measurements taken in the bearings at rated speed. This holds for any position of the crack along the shaft-line, with the exception of the few above specified positions.

It can further be noted that cracks propagate generally in positions where bending stresses are high and are magnified by stress intensity factors: this occurs exactly in the positions where high excitation has been found in the numerical simulation.

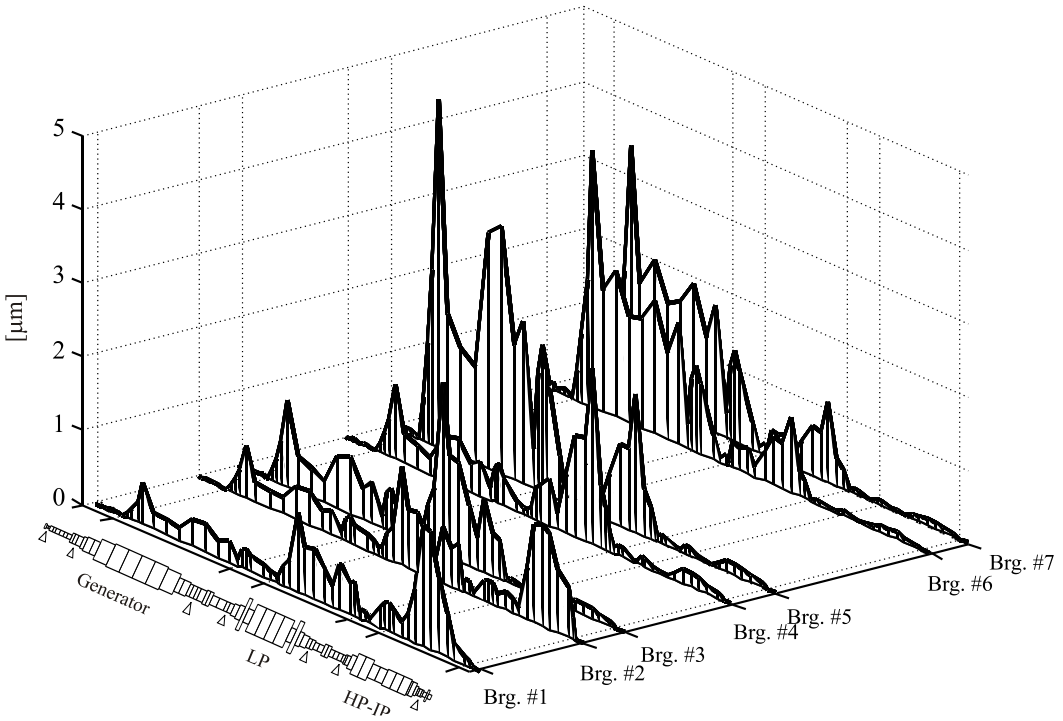

Figure 13. Waterfall plot of 2X vertical vibration amplitudes in correspondence of the bearings (at operating speed of 3000 rpm) as a function of the position of a 25% deep crack.

Figures 14 and 15 show the 1X and 2X components for crack depth of 50%. The expected increase of 1X and 2X excitations from 25% deep crack to the 50% deep crack, as calculated in for slow rotating conditions (see figure 7), is roughly 7.5 times the values of the 25% crack for the 1X component and 6.6 times for the 2X component. At rated speed, the influence of the dynamic curvature of the cracked element on the equivalent crack forces modifies the equivalent crack force values. This modification increases obviously as the crack depth increases generating higher vibrations. Therefore the calculated increase of vibrations is somewhat different from expected one. The maximum 1X and 2X amplitudes reach now respectively 63 μm and 21 μm, therefore the 1X vibrations are magnified 6.3 times and the 2X component 4.5 times, which is less than the expected values. Similar ratios are found in all other positions.

Rather deep cracks located in any position of the shaft-line, with few exceptions, generate not very large but significant 2X symptoms. Anyway, there remain still some positions in which a crack could develop and grow up to a dangerous depth, without generating measurable symptoms at rated speed. Fortunately these positions correspond to sections of the shaft-line in which the bending moment is very small (as between bearings #2 and #3) that makes the crack force excitation small but also the crack propagation difficult due to the low values of the stresses.

From these considerations it can be seen that the severity of the crack excited vibrations in the bearings, at normal operating speed, depend not only on excitation severity but also on the dynamic behaviour of the shaft-line in correspondence of the crack position and in correspondence of the bearings where the vibrations can be measured.

Much more information can be gathered if a run-down speed transient is analyzed, in which resonances can amplify the 2X symptoms.

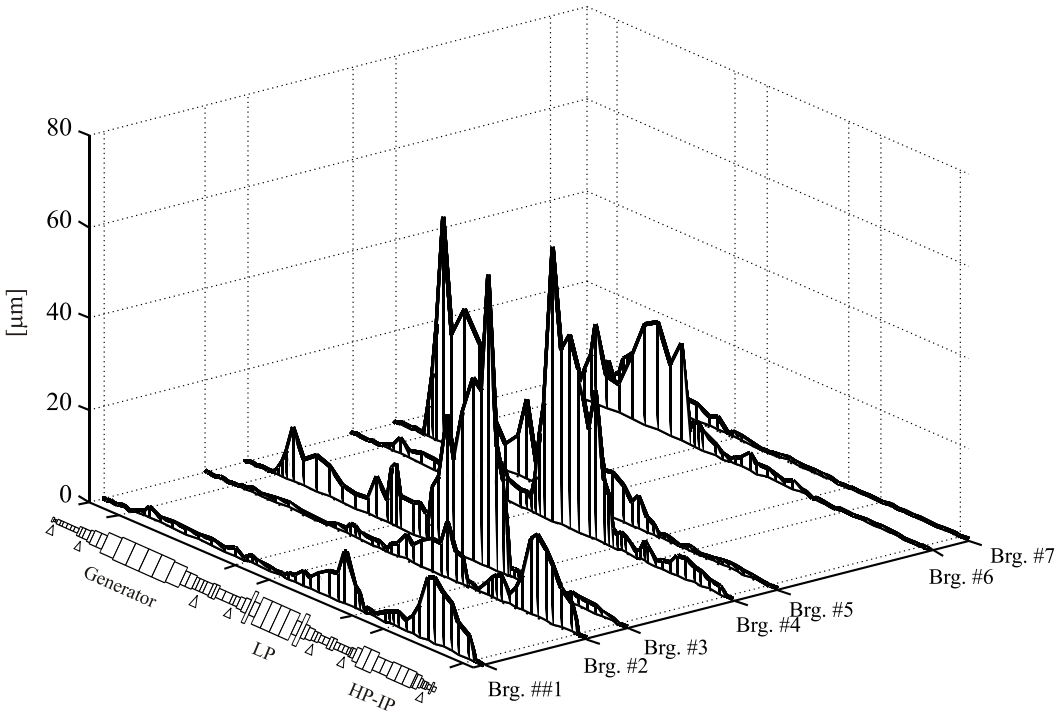

Figure 14. Waterfall plot of 1X vertical vibration amplitudes in correspondence of the bearings (at operating speed of 3000 rpm) as a function of the position of a 50% deep crack.

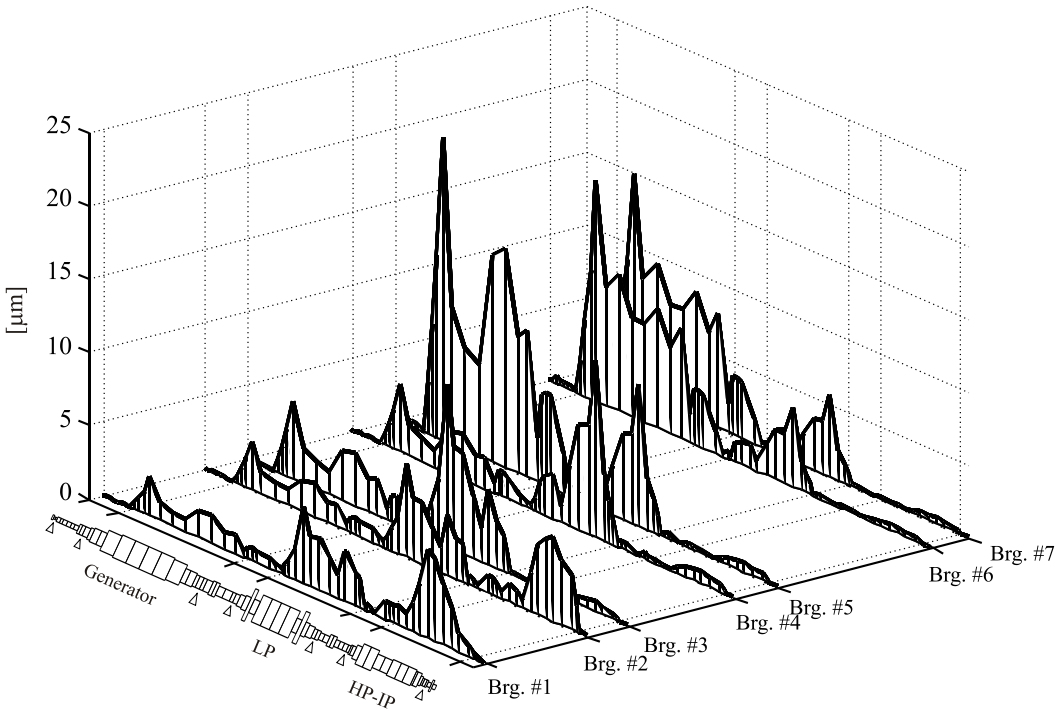

Figure 15. Waterfall plot of 2X vertical vibration amplitudes in correspondence of the bearings (at operating speed of 3000 rpm) as a function of the position of a 50% deep crack.

As an example in figure 16 the frequency response curves for the 3 harmonic components that could be measured in bearing #3 of the LP turbine, excited by a 25% crack located at mid-span, are represented. At rated speed of 3000 rpm amplitudes of 6-7 μm for the 1X component and 1-2 μm for the 2X component are found, which is in accordance with the previous simulations. These components are obviously magnified in correspondence of critical speeds. At mid-span of the LP turbine, the bending moment is maximum (strong crack force excitation) and the generalized crack force components are relevant in the first mode (at first bending critical speed) and are small in the

second mode (at its second bending critical speed) that is not excited at all. Regarding the 2X component, resonances are present at ½ of the values of first and third critical speeds. Finally also a peak at ⅓ of the first bending critical speed is clearly recognizable in the 3X component. These symptoms help strongly to identify the presence of a crack.
It should be always reminded that the excitation of 1X vibration component can be due to different causes (crack included) whereas the 2X and 3X vibration excitation are due to the stiffness asymmetry associated to the crack, if no other causes of asymmetry are present: the 2X vibration, and the 3X vibration when measurable, are the most reliable symptoms of the presence of a transverse crack in the rotating shaft.

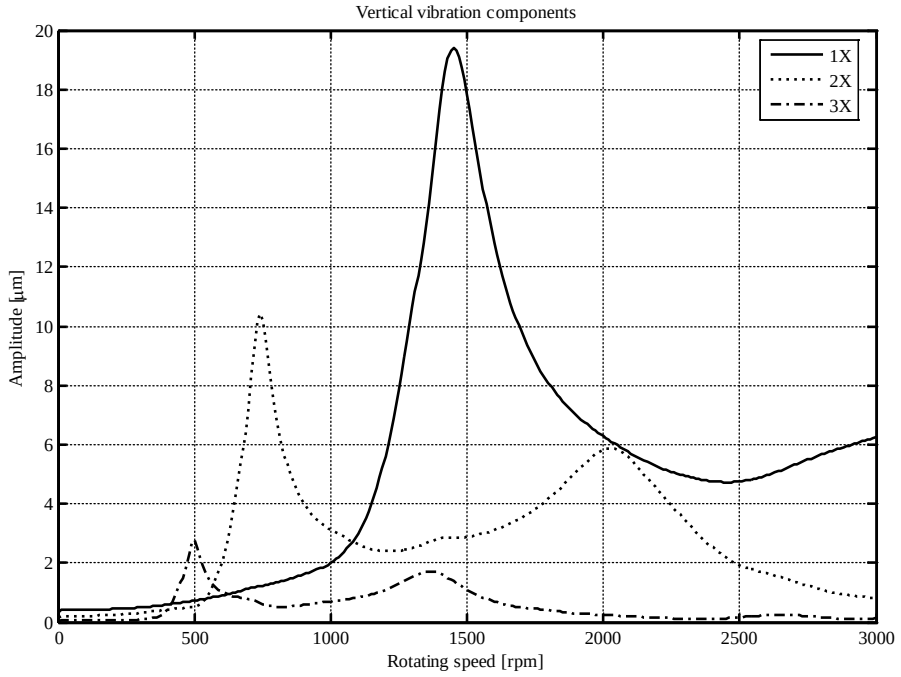

Figure 16. Vertical frequency response curves in bearing #3 for the 25% crack located at mid-span of the LP turbine.

Finally a set of calculations has been made for showing the 2X vibration amplitudes that could be measured in the bearings of the unit during a run-down transient. Only the case of the small crack, i.e. depth 25% of the diameter, and the vibrations in one bearing are shown as an example when the crack is located successively in all different beam elements of the unit model. The resulting waterfall diagram of the vibration amplitudes in vertical direction obtained in bearing #4 is shown in figure 17. The maximum vibration amplitudes are obtained in correspondence of the first natural frequencies of LP turbine and of generator and are about 10 μm. As can be seen from figure 17, bearing #4 is sensitive to cracks which develop in the main bodies of LP turbine and generator but is insensitive to cracks that develop in HP-IP turbine or in the exciter of the generator. Their symptoms could be measured in other bearings.
From this analysis it results once again that the most reliable symptoms of a developing crack are the 2X components that are excited in resonance corresponding to the first natural frequencies of the different shafts during a run-down transient of the unit.

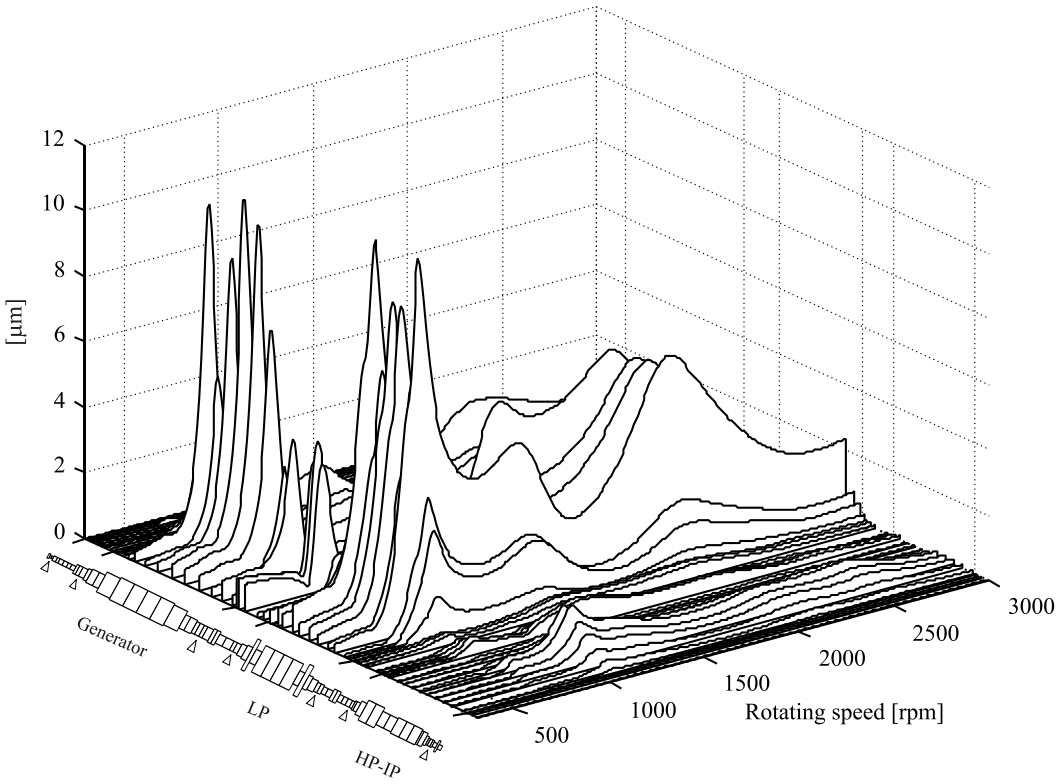

Figure 17. 2X vibration amplitudes in vertical direction in bearing #4 during a run-down transient as function of different crack positions (crack depth 25%).

6. Conclusions

The excitation of vibrations in correspondence of the bearings of cracked turbogenerator units, where generally shaft vibrations are measured, is analysed. All the positions of the crack along the shaftline are considered in order to evaluate the effects on the dynamic response at rated speed and during run down transients.

Summarizing, the following results emerge from the analysis:

i. crack forces depend on depth and are proportional to the static bending moment divided by the third power of the shaft diameter;
ii. the excitation of maximum vibrations at a given rotating speed per unit crack force occurs when the corresponding mode shape presents high curvature in correspondence of the crack position;
iii. the maximum response occurs obviously in resonant conditions with 1X, 2X and 3X critical speeds.

Difficulties in detecting small cracks in rated speed conditions are highlighted. The vibration trend at the increasing crack depths is derived, and the advantages of considering run down transients instead of rated speed conditions are emphasized. These results could contribute consistently to an assessment of crack excited vibrations and to the possibilities of detecting cracks in turbogenerator units from standard vibration measurement and monitoring systems.

References

[1] Paris PC, Erdogan F (1960) A critical analysis of crack propagation laws. Journal of Basic Engineering, 85, 528-534.

[2] DeForest DH, Grobel LP, Schabtach C, Seguin BR (1957) Investigation of the Generator Rotor Burst at the Pittsburg Station of the Pacific Gas and Electric Company. ASME Paper No. 57-PWR-12, 3-14.

[3] Ishida Y (2008) Cracked Rotors : Industrial Machine Case Histories and Nonlinear Effects Shown by Simple Jeffcott Rotor. Mechanical Systems and Signal Processing, 22(4), 805-817.
[4] Rankin AW, Seguin BR (1956) Report of the Investigation of the Turbine Wheel Fracture at Tanners Creek. Transactions of the ASME, 78(10), 1527.
[5] Schabtach C, Fogleman EL, Rankin AW, Winne DH (1956) Report of the Investigation of Two Generator Rotor Fractures. Transactions of the ASME, 78(10), 1567.
[6] Emmert HD, (1956) Investigation of Large Steam-Turbine Spindle Failure. Transactions of the ASME,78-10(1956-10), 1547-1565.
[7] Whyte RR (1975) Engineering Progress Through Trouble. The Institution of Mechanical Engineers, Chap.10.
[8] Yoshida M (1976) Steam Turbine Rotor Accidents and its Countermeasure. Turbomachinery, 4-11, 728.
[9] Jack AR, Paterson AN (1976) Cracking in 500MW LP Rotor Shafts, 1st Mech. Eng. Conference, The Influence of the Environment on Fatigue.
[10] Muszynska A (1982) Shaft Crack Detection. 7th Machinery Dynamics Seminar, Edmonton, Canada.
[11] Laws CW (1986) A Brief History of Cracked Rotor Saves – Turbine Generators in the U.K. Rated 60MW to 660MW (1971-1981). Bently Rotor Dynamics Co Seminar on Shaft Crack Detection, Atlanta GA, USA.
[12] Ziebarth H, Baumgartner RJ (1981) Early Detection of Cross-Sectional Rotor Cracks by Turbine Shaft Vibration Monitoring Techniques. ASME Paper 81-JPGC-PWR-26.
[13] Papadopoulos CA, Dimarogonas W (1988) Stability of Cracked Rotors in the Coupled Vibration Mode. ASME Journal of Vibrations, Acoustics, Stress and Reliability in Design, 110, 356-359.
[14] United States Nuclear Regulatory Commission (1986) Information Notice 86-19: Reactor Coolant Pump Shaft Failure at Crystal River.
[15] United States Nuclear Regulatory Commission (1989) Information Notice 89-15: Second Reactor Coolant Pump Shaft Failure at Crystal River.
[16] The Tampa Tribune (1989), January 20, 14-B.
[17] Maxwell JH, Rosario DA (2001) Using modelling to predict vibration from a shaft crack. Condition Monitoring and Diagnostic Engineering Management (COMADEM 2001), Elsevier, 243-250.
[18] United States Nuclear Regulatory Commission (2005) Information Notice 2005-08: Monitoring Vibration to Detect Circumferential Cracking of Reactor Coolant Pump and Reactor Recirculation Pump Shafts.
[19] Inagaki T, Hirabayashi M (1990) Transverse Vibrations of Cracked Rotors (Examples of Crack Detection and Vibration Analysis). Transactions of JSME, 56-523, 582.
[20] Sanderson AFP (1992) The Vibration Behaviour of a Large Steam Turbine Generator During Crack Propagation Through the Generator Rotor. IMechE International Conference on Vibrations in Rotating Machinery, Bath, UK, paper C432/102, 263-273.
[21] Schöllhorn K, Ebi G, Steigleder K (1993) Frettinganrisse in einem 936-MW Turbogeneratorrotor. VGB Kraftwerkstechnik, 73(4), 340-344.
[22] Bicego V, Lucon E, Rinaldi C, Crudeli R (1999) Failure analysis of a generator rotor with a deep crack detected during operation: Fractographic and fracture mechanics approach. Nuclear Engineering and Design, 188(2), 173-183.
[23] Stoisser CM, Audebert S (2008) A comprehensive theoretical, numerical and experimental approach for crack detection in power plant rotating machinery. Mechanical Systems and Signal Processing, 22(4), 818-844.
[24] Gasch R (1976) Dynamic Behaviour of a Simple Rotor with a Cross-sectional Crack. IMECHE Conference Vibrations in Rotating Machinery, paper 178/76, 123-128.
[25] Mayes IW, Davies WGR (1976) The vibrational behaviour of a rotating shaft system containing a transverse crack. IMECHE Conference Vibrations in Rotating Machinery, paper 168/76, 53-64.
[26] Bachschmid N, Pennacchi P, Tanzi E (2008) Some remarks on breathing mechanism, on non-linear effects and on slant and helicoidal cracks. Mechanical Systems and Signal Processing, 22(4), 879-904.
[27] Bachschmid N, Tanzi E (2003) Stresses and Strains in Correspondence of a Transverse Crack in a Shaft: Effect of Crack Closure. International Conference on Fatigue Crack Paths (FCP 2003), Parma, Sept. 2003, 1-10.
[28] Bachschmid N, Tanzi E (2006) Effect of shear forces on cracked beam deflections. International Conference on Fatigue Crack Paths (FCP 2006), Parma, Sept. 2006, 1-10.